Inductively coupled plasmas sustained by an internal oscillating current

E. L. Tsakadze, K. N. Ostrikov, S. Xu, R. Storer, and H. Sugai

Citation: J. Appl. Phys. **91**, 1804 (2002); doi: 10.1063/1.1430893
View online: http://dx.doi.org/10.1063/1.1430893
View Table of Contents: http://jap.aip.org/resource/1/JAPIAU/v91/i4
Published by the American Institute of Physics.

Inductively coupled plasmas sustained by an internal oscillating current

E. L. Tsakadze
Plasma Sources and Applications Centre, NIE, Nanyang Technological University, 1 Nanyang Walk, 637616 Singapore, Singapore

K. N. Ostrikov[a)]
Department of Electrical Engineering, Nagoya University, Furo-cho, Chikusa-ku, Nagoya 464-8603, Japan, Plasma Sources and Applications Centre, NIE, Nanyang Technological University, 1 Nanyang Walk, 637616 Singapore, and School of Chemistry, Physics and Earth Sciences, The Flinders University of South Australia, GPO Box 2100, Adelaide SA 5001, Australia

S. Xu[b)]
Plasma Sources and Applications Centre, NIE, Nanyang Technological University, 1 Nanyang Walk, 637616 Singapore

R. Storer
School of Chemistry, Physics and Earth Sciences, The Flinders University of South Australia, GPO Box 2100, Adelaide SA 5001, Australia

H. Sugai
Department of Electrical Engineering, Nagoya University, Furo-cho, Chikusa-ku, Nagoya 464-8603, Japan

(Received 11 June 2001; accepted for publication 3 November 2001)

A global electromagnetic model of an inductively coupled plasma sustained by an internal oscillating current sheet in a cylindrical metal vessel is developed. The electromagnetic field structure, profiles of the rf power transferred to the plasma electrons, electron/ion number density, and working points of the discharge are studied, by invoking particle and power balance. It is revealed that the internal rf current with spatially invariable phase significantly improves the radial uniformity of the electromagnetic fields and the power density in the chamber as compared with conventional plasma sources with external flat spiral inductive coils. This configuration offers the possibility of controlling the rf power deposition in the azimuthal direction. © *2002 American Institute of Physics.* [DOI: 10.1063/1.1430893]

I. INTRODUCTION

There has been a great deal of interest in high-density, low-temperature plasma sources for various applications.[1–4] Inductively coupled plasma (ICP) sources featuring high (10^{11}–10^{12} cm^{-3}) ion densities and low plasma potentials have proved to be very efficient in the generation of large-area and large-volume plasmas for fabrication of unique nanostructures, synthesis, and processing of advanced materials and ultrafine selective etching of semiconductor wafers.[5–11] The unmagnetized ICPs are generated by time-varying electromagnetic fields excited by rf currents driven in external or internal coils powered by an rf generator through a matching circuit.[5,7,12,13] However, the uniformity of the electromagnetic fields and rf power density, which is a key factor for plasma processing applications, still deserves substantial improvement.[14]

Recently a few attempts to improve the uniformity of the power deposition, by modifying the coil configuration and adjusting the rf power/plasma coupling, have been made. In particular, a series connection of parallel conductors embedded in the plasma inside thin quartz tubes has proved to be capable of large-area, fairly uniform plasma production.[15] Another antenna configuration with a six-turn segmented coil, where five inner segments are connected in parallel with the external sixth segment through a variable capacitor, has also been reported.[16] In this scheme, one can achieve a high degree of uniformity of the electron/ion number density by proper adjustment of the power/plasma coupling.

The uniformity of the electromagnetic fields and rf power transferred to the plasma electrons can also be improved by excitation of the internal rf current with spatially-varying phase.[17] A similar principle, in combination with vertical steady magnetic fields, has been used in rotating magnetic field current-drive experiments.[18] Furthermore, schemes with internally driven rf currents usually achieve plasma production with lower powers than those with external coils.[19,20] Indeed, in conventional external-coil schemes useless rf fields are usually generated outside the chamber.[17] The results of computation show that by using an internal rotating current (IRC), one can improve the uniformity of power density and simultaneously minimize power consumption.[17]

An obvious drawback of the conventional ICP source with an external flat spiral coil is its inefficiency for upscal-

[a)]Also with: Department of Electrical and Electronic Engineering, Nanyang Technological University, 639798 Singapore, Singapore.
[b)]Author to whom correspondence should be addressed; electronic mail: syxu@nie.edu.sg

ing due to parasitic standing-wave effects.[14,15] In addition, larger plasma reactors would require enlarged fused silica windows, which have to be made thick enough to withstand huge pressure loads. Hence, the relative power coupling and cost efficiency of upscaled conventional ICP sources could dramatically decrease. In this regard, fully metal chambers with internal rf power input seem advantageous in comparison with the external-coil devices.

In this article, we consider high-density plasma production by an internal oscillating current (IOC) in a fully metal vacuum chamber and compare the results with the ICP and IRC-generated plasma (IRCGP) cases. The IOC principle has earlier been tested for the efficient steady-state current drive in compact spherical tori.[21]

Using the basic electromagnetic equations and conservation laws, the distribution of electromagnetic field in the chamber, the efficiency of power deposition, and the spatially averaged plasma density are computed. It is shown that nonuniformity of the rf power density and electromagnetic fields, a troublesome problem peculiar to the ICP sources, can be overcome by exciting a spatially invariable (unidirectional) current sheet inside a cylindrical metal vessel.

The article is organized as follows. In Sec. II the spatial distribution of the electromagnetic field in the cylindrical resonator with an internal oscillating rf current is studied. In Sec. III the power transferred to the IOC generated plasma (IOCGP) is computed and visualized. In Sec. IV the power and particle balance are considered and approximate profiles of the plasma density are obtained. The working points of a low-pressure argon discharge are calculated in Sec. V. The results obtained and the limitations of our analysis are discussed in Sec. VI. A brief summary of this work is given in Sec. VII.

II. ELECTROMAGNETIC FIELD CONFIGURATION

In this section the distribution of the electromagnetic fields within the cylindrical metal vessel of internal radius R and length $L+\mathcal{L}$ is studied. The chamber top is located at $z=-\mathcal{L}$, and the bottom is at $z=L$. We consider the plasma generated by a rf current sheet with spatially constant phase which is uniformly distributed over the cylindrical cross section $z=0$:

$$I_{\mathrm{RF}}=I_0\exp(-i\omega t)[\cos(\phi)\hat{r}-\sin(\phi)\hat{\phi}]. \tag{1}$$

This is a unidirectional oscillating rf current depicted in Fig. 1 at different moments of time. Here, $\hat{r}$ and $\hat{\phi}$ are unit vectors in the radial and azimuthal directions and I_0 and ω are the rf current amplitude and frequency, respectively. In the calculation of the electromagnetic fields and rf power density, we assume that a spatially uniform plasma with different densities n_1 and n_2 exists in the volumes above $(-\mathcal{L}<z<0)$, and beneath $(0<z<L)$ the current sheet, respectively. We note that the above current is a practical alternative to the internal rotating (spatially varying) current $I_{\mathrm{RF}}=I_0\exp[-i(\omega t-\phi)](\hat{r}+i\hat{\phi})$, considered in Ref. 17.

The electromagnetic fields are computed using the set of Maxwell's equations[22]

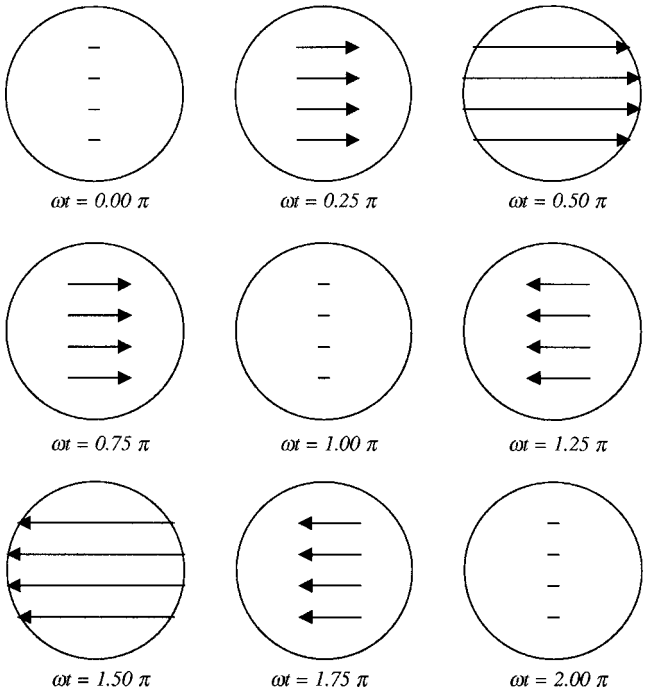

FIG. 1. Sketch of the internal oscillating rf current.

$$\nabla\times\mathbf{E}_j=-\frac{1}{c}\frac{\partial\mathbf{H}_j}{\partial t}, \tag{2}$$

$$\nabla\times\mathbf{H}_j=\frac{1}{c}\frac{\partial(\varepsilon_j\mathbf{E}_j)}{\partial t}, \tag{3}$$

where $\mathbf{E}_j$ and $\mathbf{H}_j$ are the electric and magnetic fields in the two different plasma volumes $(j=1,2)$, respectively. Here, $\varepsilon_j=1-\omega_{pj}^2/[\omega(\omega+i\nu_{ej})]$ is the permittivity of the cold uniform plasma, ω_{pj} is the electron plasma frequency, and ν_{ej} is the effective rate of electron–neutral collisions. We consider the transverse-electric (TE) solutions of Eqs. (2)–(3) with the components of the electromagnetic field $\mathbf{E}=(E_r,E_\phi,0)$ and $\mathbf{H}=(H_r,H_\phi,H_z)$. Applying the electrodynamic boundary conditions at $z=0,-\mathcal{L},L$, and $r=R$,[22] and focusing on field and plasma parameters in the volume $0<z<L$, one can obtain the following TE solution:

$$H_r^{(2)}=\sin(\phi)\sum_{n=1}^{\infty}\gamma_n^{(2)}\kappa_n\xi_1^{(2)}(z)\frac{\partial}{\partial r}J_1(\Upsilon_{1n}r), \tag{4}$$

$$H_\phi^{(2)}=-\cos(\phi)\frac{1}{r}\sum_{n=1}^{\infty}\gamma_n^{(2)}\kappa_n\xi_1^{(2)}(z)J_1(\Upsilon_{1n}r), \tag{5}$$

$$H_z^{(2)}=\sin(\phi)\sum_{n=1}^{\infty}\kappa_n\Upsilon_{1n}^2\xi_2^{(2)}(z)J_1(\Upsilon_{1n}r), \tag{6}$$

$$E_r^{(2)}=i\cos(\phi)\frac{\omega}{cr}\sum_{n=1}^{\infty}\kappa_n\xi_2^{(2)}(z)J_1(\Upsilon_{1n}r), \tag{7}$$

$$E_\phi^{(2)}=-i\sin(\phi)\frac{\omega}{c}\sum_{n=1}^{\infty}\kappa_n\xi_2^{(2)}(z)\frac{\partial}{\partial r}J_1(\Upsilon_{1n}r), \tag{8}$$

where $\kappa_n=\vartheta_n/D_n(\mathrm{TE})$, $\Upsilon_{1n}=\rho'_{1n}/R$,

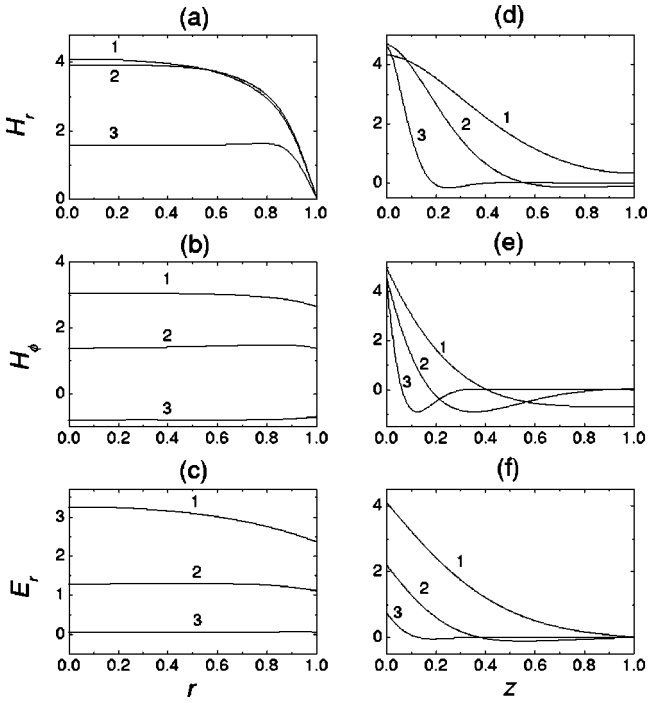

FIG. 2. Nondimensional profiles of H_r, H_ϕ, and $E_r\times 10^3$ field components (multiplied by -1) for $\nu_{e2}/\omega=35$, $\nu_{e2}/\nu_{e1}=2.0$, and $\omega_{p2}/\omega_{p1}=1.5$. (a)–(c) stand for radial profiles at $z/L=0.1$ and $\phi=45°$, while (e)–(f) for axial profiles at $r/R=0.2$ and the same azimuthal position. Curves 1–3 correspond to $n_e=3\times10^{11}$, 10^{12}, and 8×10^{12} cm^{-3}, respectively.

$$\xi_1^{(2)}(z)=\cosh[\gamma_n^{(2)}(L-z)]/\sinh(\gamma_n^{(2)}L),$$

$$\xi_2^{(2)}(z)=\sinh[\gamma_n^{(2)}(L-z)]/\sinh(\gamma_n^{(2)}L),$$

$$\vartheta_n=\int_0^R rJ_1(\Upsilon_{1n}r)f(r)dr \Big/ \int_0^R rJ_1^2(\Upsilon_{1n}r)dr,$$

$$D_n(\mathrm{TE})=\gamma_n^{(1)}\coth(\gamma_n^{(1)}\mathcal{L})+\gamma_n^{(2)}\coth(\gamma_n^{(2)}L),$$

is the dispersion relation for the TE electromagnetic field in the plasma-filled cylindrical metal resonator with radius R and length $L+\mathcal{L}$, $\gamma_n^{(1,2)}=[\Upsilon_{1n}^2-(\omega/c)^2\varepsilon_{(1,2)}]^{1/2}$ is the inverse field penetration length, $\partial J_1(\rho'_{1n})/\partial r=0$, $f(r)=(4\pi/c)\mathcal{J}r$, and $\mathcal{J}=I_0/2R$ is a surface current per unit diameter. Here, the superscripts 1 and 2 correspond to the volumes $-\mathcal{L}<z<0$ and $0<z<L$, respectively.

Figure 2 depicts the radial and axial profiles of H_r, H_ϕ, and E_r components of the electromagnetic field in the chamber for different plasma densities, azimuthal angle $\phi=45^0$ and given axial and radial position at $t=0$. Similar dependence for the axial magnetic and azimuthal electric field components is displayed in Fig. 3 for the same plasma densities and another azimuthal position ($\phi=90^0$).

The plasma parameters (Table I) have been taken as representative values in the experiments on low-frequency ($\sim$0.5 MHz) ICPs.[10,23–25] Figures 2–3 show that the electromagnetic field generated by the internal oscillating current is highly uniform in radial direction, especially in the vicinity of the chamber walls. We note that all field components, except for the axial magnetic field [Figs. 3(a) and 3(c)], have maximum values near the chamber axis. The vanishing of the field at the chamber walls is consistent with conventional

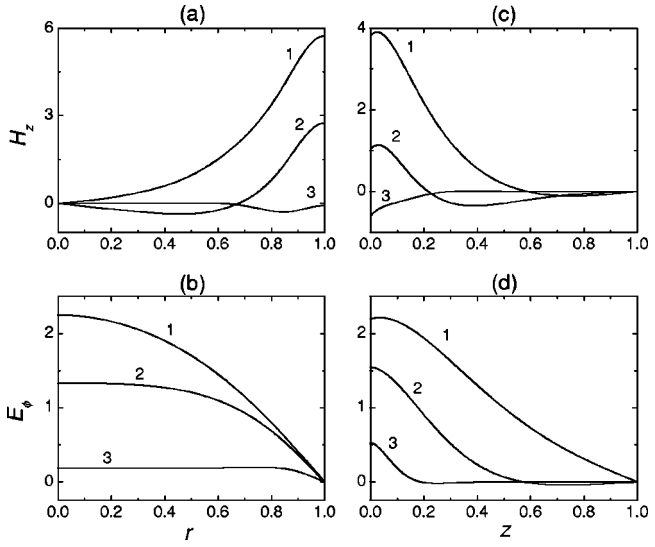

FIG. 3. Same as in Fig. 2 for H_z and $E_\phi\times10^3$, $\phi=90°$. In (c) and (d), radial position r/R is 0.8 and 0.2, respectively.

boundary conditions at ideally conducting metal surfaces.[22] The electromagnetic field components also feature maxima near the excitation source ($z=0$) and diminish toward the bottom of the vessel. It is also evident that, as the plasma density increases, the electromagnetic field becomes more and more localized near the plane $z=0$, which is obviously attributed to the "skin effect"[2] essential for most rf plasmas.

We now compare the dependence of the TE field penetration length into the chamber on the plasma parameters in the IOCGP and the ICP. For simplicity, from this point onward the ICP means the ICPs generated in the conventional configuration with an external flat spiral coil at $z=-d$, where d is a thickness of the dielectric window separating the plasma from the coil. In reality, d includes a thick air gap inbetween the coil holder and a quartz window.[10,23–25] It is worth mentioning that the field penetration length is an important characteristic of rf power deposition.[2] Figure 4 shows the ratio $q=(\gamma_1^{(2)}/\gamma_0)^{-1}$ of the field penetration depths in

TABLE I. Main parameters and typical values.

Parameter	Notation	Value
Electron temperature	T_e	1.5–2.5 eV
Ion temperature	T_i	0.026 eV
Temperature of neutrals	T_n	0.026 eV
Gas pressure (Ar)	p_0	30–100 mTorr
Plasma density	n_e	10^9–7×10^{12} cm^{-3}
Absorbed rf power	P_p	0.1–1 kW
Window dielectric constant (ICP)	ϵ_d	4
Window thickness (ICP)	d	1.6 cm
Chamber length (inner)	L	20 cm
Chamber radius (inner)	R	16 cm
Generator frequency	$\omega/2\pi$	500 kHz
Amplitude of rf current	I_0	15–25 A
Ionization threshold (Ar)	$\mathcal{E}_i$	15.76 eV
4s excitation threshold (Ar)	$\mathcal{E}_{4s}$	11.5 eV
4p excitation threshold (Ar)	$\mathcal{E}_{4p}$	13.2 eV
Ion mass (Ar)	m_i	$1836\times40\times m_e$
Cross section (i–n collisions)	σ_{in}	10^{-14}–10^{-15} cm^2

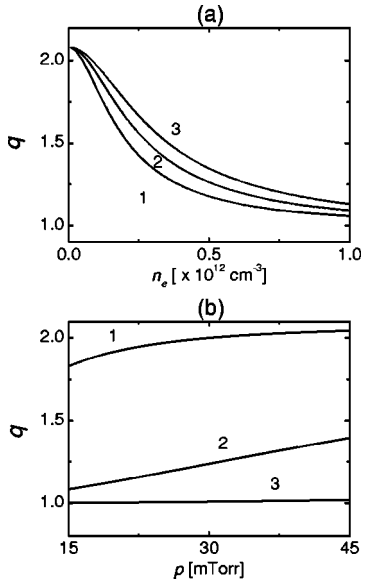

FIG. 4. Ratio of the rf field penetration lengths q vs plasma density (a), and gas filling pressure (b). In (a), curves 1–3 correspond to gas pressures $p_0=15$, 20, and 25 mTorr, respectively. In (b), curves 1–3 are plotted for $n_e=10^{11}$, 8×10^{11}, and 5×10^{12} cm^{-3}, respectively.

the two configurations (IOC and ICP) as a function of plasma density for different gas pressures [Fig. 4(a)] and *versus* gas pressure for different plasma densities [Fig. 4(b)]. Here $\gamma_0=[\Upsilon_{01}^2-(\omega/c)^2\varepsilon_2]^{1/2}$ is the inverse field penetration depth in the ICP source, $\Upsilon_{01}=\rho'_{01}/R$, and $dJ_0(\rho'_{01})/dx=0$.[10,26] From Fig. 4 one can see that at plasma densities $n_e<10^{12}$ cm^{-3}, the value of $(\gamma_1^{(2)})^{-1}$ can be up to two times larger than γ_0^{-1}. However, at higher electron number densities the difference between the two field penetration lengths becomes small. Hence, the IOC configuration appears to be more advantageous compared to the ICP source in terms of better TE field penetration into the chamber at intermediate ($n_e\sim10^{10}$–10^{11} cm^{-3}) plasma densities.

The distribution of the IOC-generated magnetic field in the poloidal (r,z) cross section is plotted in Fig. 5 for rarefied ($n_e\sim10^9$ cm^{-3}) and dense ($n_e\sim10^{12}$ cm^{-3}) plasmas. It is evident that at higher plasma densities the field is localized mainly in the vicinity of the current plane. Figure 5 also confirms the high degree of radial uniformity of the electromagnetic fields generated by the IOC. Moreover, as follows from Figs. 2–5, the radial uniformity of the electromagnetic fields in the IOCGP is indeed better than in the ICP.

III. rf POWER DENSITY

We now turn our attention to computation of the power transferred to the plasma electrons and investigate the dependence of the rf power density on the plasma and discharge control parameters. Contrary to the ICP case featuring a sole electric field component E_ϕ, the IOC generates an additional radial electric field E_r and hence the azimuthal magnetic field B_ϕ. An additional electric field component will definitely modify the power absorbed by highly mobile plasma electrons and the power balance in the chamber in general. Possible implications of generation of the azimuthal magnetic field component are discussed in Sec. VI. It is remarkable that the electrons are predominantly heated in a narrow power absorption region, which is normally on the order of the field penetration length γ_1^{-1}. The neutrals can be excited and ionized through electron impact processes. Using the fluid approach, for the power deposited into the plasma volume $0<z<L$, one can obtain

$$W_p=\frac{1}{4\pi}\int_V \mathrm{Re}[\sigma^{(2)}]|\mathbf{E}^{(2)}|^2\,dV, \tag{9}$$

where $\sigma^{(2)}=\omega_{p2}^2/4\pi(\nu_{e2}-i\omega)$ is the plasma conductivity, $dV=2\pi r\,dr\,d\phi$, and $|\mathbf{E}^{(2)}|^2=[\mathrm{Re}(E_r^{(2)})]^2+[\mathrm{Im}(E_r^{(2)})]^2+[\mathrm{Re}(E_\phi^{(2)})]^2+[\mathrm{Im}(E_\phi^{(2)})]^2$. Note that in the ICP case $|\mathbf{E}_{\mathrm{ICP}}^{(2)}|^2=[\mathrm{Re}(E_\phi^{(2)})]^2+[\mathrm{Im}(E_\phi^{(2)})]^2$. Equation (9) will further be used in computation of the discharge working points.

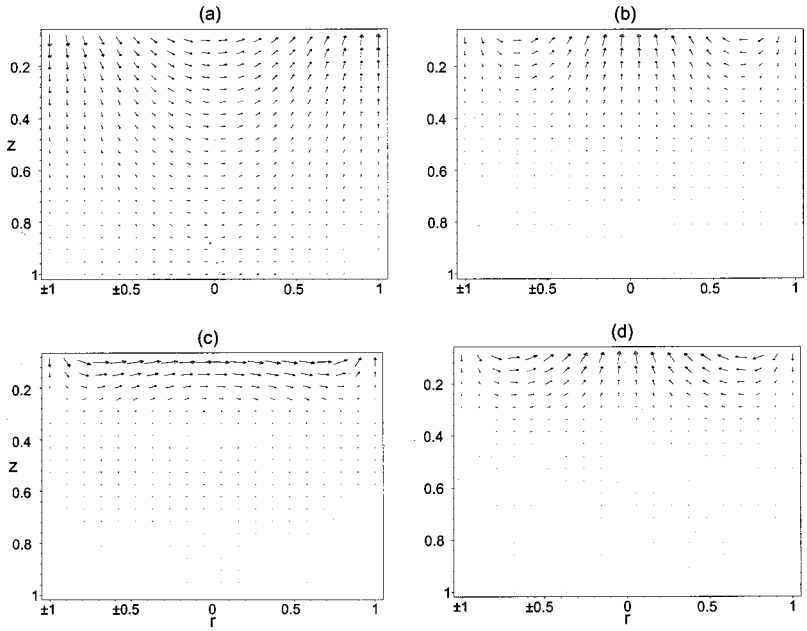

FIG. 5. Magnetic field lines in poloidal $\phi=90°$ cross section for rarefied [$\sim10^9$ cm^{-3}, diagrams (a) and (b)] and dense [$\sim10^{12}$ cm^{-3}, diagrams (c) and (d)] plasmas generated in the IOC (a),(c) and ICP (b),(d) configurations.

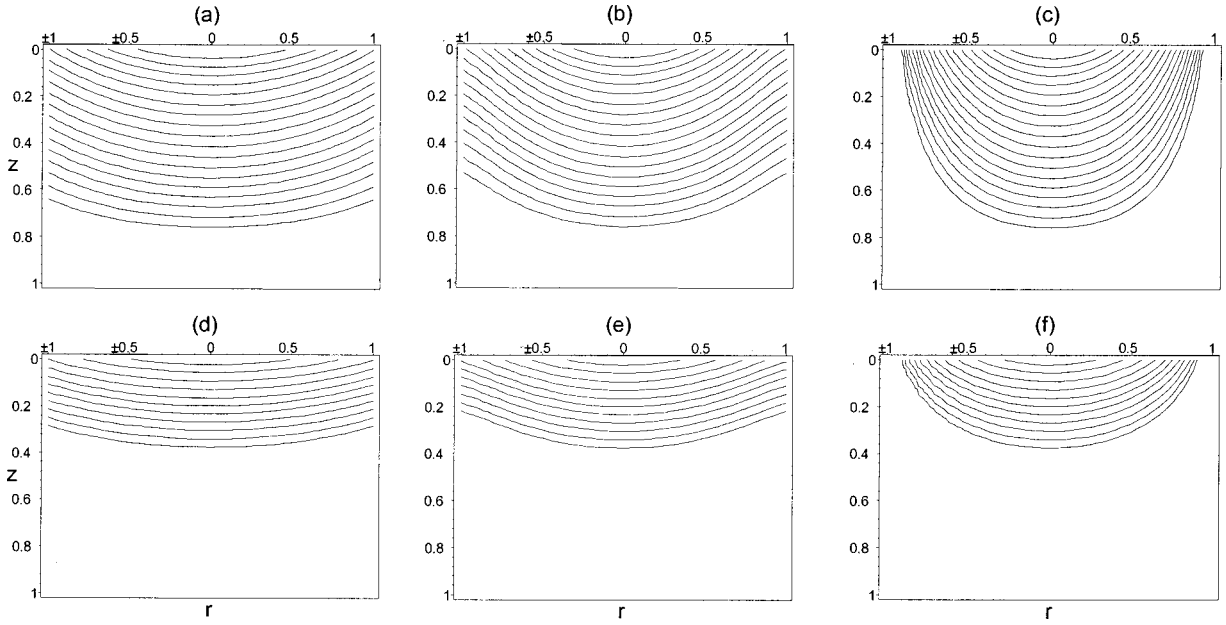

FIG. 6. Contours of the rf power density in the chamber filled by rarefied (a),(b),(c) and dense (d),(e),(f) IOC-generated plasmas plotted for $\phi=0°$ (a),(d), $\phi=45°$ (b),(e), and $\phi=90°$ (c),(f). Plasma densities are the same as in Fig. 5.

The distribution of the rf power transferred to the plasma electrons over the poloidal cross section is visualized in Figs. 6 and 7 for 500 kHz IOC-driven rarefied ($n_e \sim 10^9$ cm^{-3}) and dense ($n_e \sim 10^{12}$ cm^{-3}) plasmas. For comparison, we have also computed similar distributions for the IRCGP and ICP in the chamber with the same geometrical sizes, plasma parameters, and rf frequency.

The remarkable difference of the IOC case from the IRC and ICP configurations is in azimuthal profiles of the rf power density W_{pV}. Indeed, the IRC and ICP devices produce axially symmetric profiles of W_{pV}, while in the IOC configuration the power absorbed by the plasma electrons features a clearly resolved dipolar azimuthal profile (Fig. 8). This gives the possibility of controlling the power deposition in processes requiring azimuthal profiling of the film thickness or etch rate.[1] Further comparison reveals deeper power deposition in the IOC and IRC configurations in comparison with the ICP. Figures 8 and 9 also elucidate the high degree of radial uniformity of the rf power density in the IOC and IRC schemes.

It is worthwhile to mention that in a conventional ICP the power absorbed by the plasma electrons appears to be strongly nonuniform near the chamber axis [Figs. 7(a) and 9(b)]. Similar nonuniformity in the power contours in low-frequency ICPs have been reported earlier.[10,25,27] On the other hand, such a nonuniformity can be eliminated by gen-

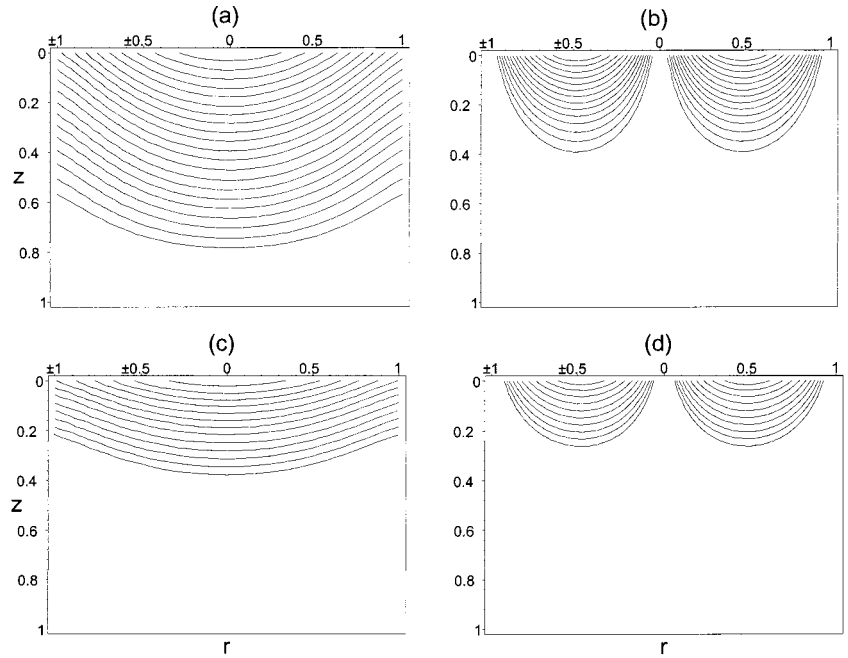

FIG. 7. Same as in Fig. 6 for the IRC (a),(b) and ICP (c),(d) geometries.

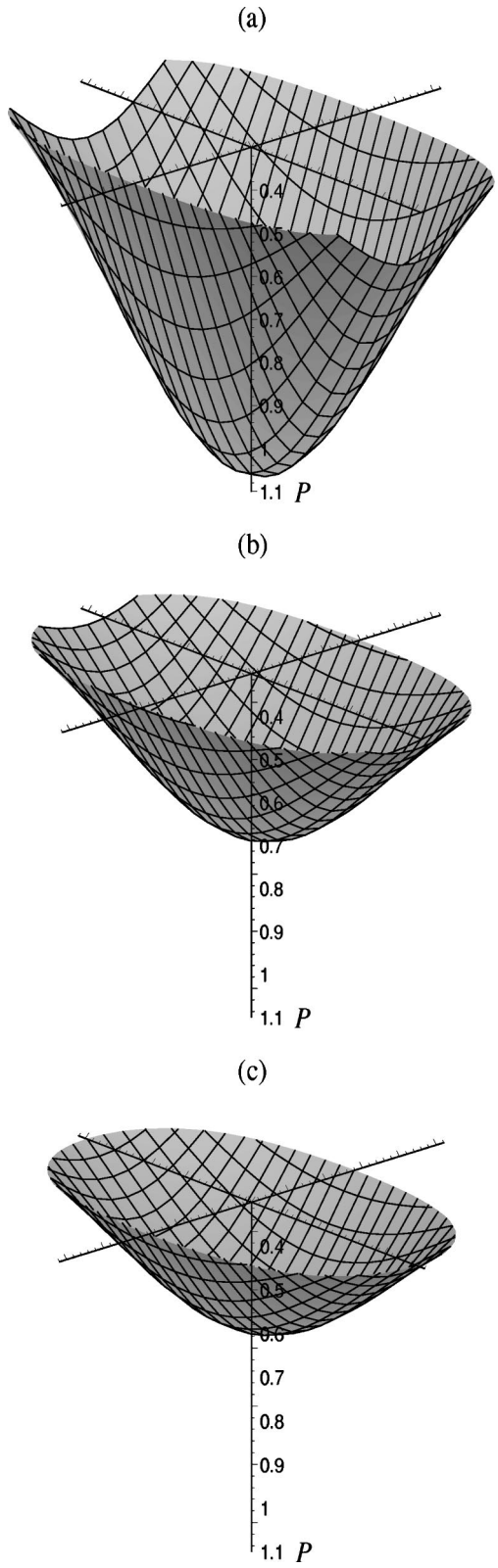

FIG. 8. Three-dimensional (3D) plot of the rf power density deposited by the IOC for $n_e = 10^{11}$ cm^{-3} and gas pressure $p_0 = 20$ mTorr (a), 25 mTorr (b), 30 mTorr, and (c), respectively.

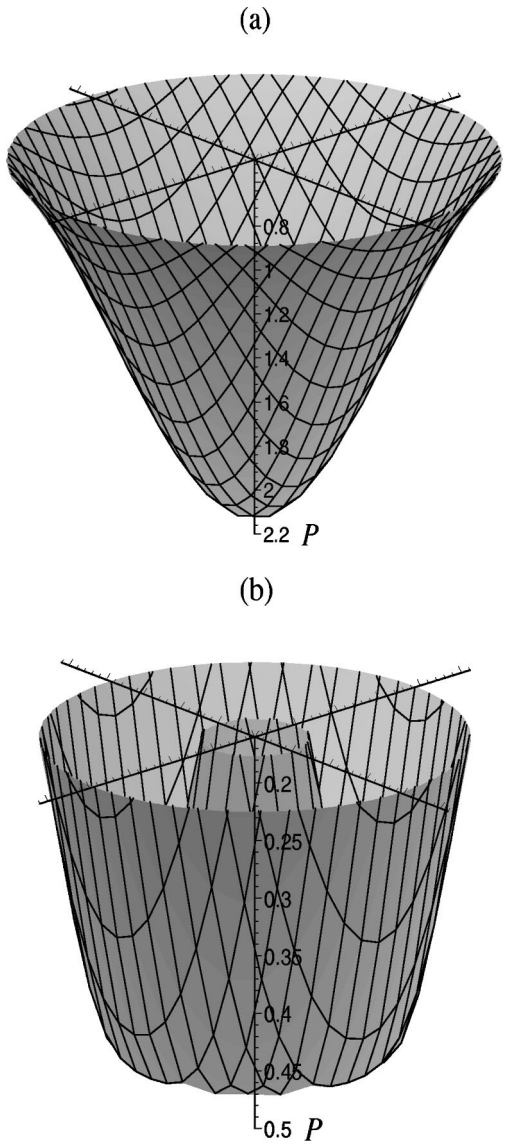

FIG. 9. Same as in Fig. 8 for the IRC (a) and ICP (b) geometries and $p_0 = 20$ mTorr.

erating the internal rf curents with spatially constant (Figs. 6 and 8) or spatially varying [Figs. 7(b), 7(d), and 9(b)] phases. Furthermore, the radial uniformity of power deposition into the plasma improves at higher electron/ion number densities. The difference between the IOC and IRC schemes appears to be in azimuthal profiles and maximal absolute values of power density, the latter being twice higher in the IRC case under the same I_0, chamber sizes and plasma parameters.

Figure 10 shows the nondimensional total power absorbed by the plasma $W_p^{\mathrm{nd}} = W_p(c/R\mathcal{J}\sqrt{\omega})^2$ as a function of the plasma density and gas pressure. It should be noted that W_p rises with pressure, which is consistent with Eq. (9). At low plasma densities, the power absorbed by the plasma increases with n_e, while at higher densities it starts to decline when the electron/ion number density reaches $n_e \sim 5\times 10^{11}$ cm^{-3}. From Fig. 10 one can see that the critical plasma density increases with pressure, being $n_e \sim 6.3\times 10^{11}$ cm^{-3} at $p_0 = 30$ mTorr. A similar tendency has previously been reported for the IRC configuration.[17]

IV. POWER AND PARTICLE BALANCE

Here we apply the power and particle conservation equations to compute the minimal rf power necessary to sustain

the discharge with the required electron/ion number density as a function of operating gas pressure and other control parameters. In these calculations we assume the same size of the vacuum chamber and the rf frequency as in low-frequency ICPs ($R=16$ cm, $L=20$ cm, and $\omega/2\pi=500$ kHz).[23,24] In the steady state we have

$$W_p = W_{\text{loss}}, \tag{10}$$

$$\nabla(D_a \nabla n_e) - \nu_i n_e = 0, \tag{11}$$

where $W_{\text{loss}}=n_v V_p \theta_p$ is the electron power loss to sustain the plasma with the spatially averaged density n_v in the volume V_p

$$\theta_p = e[\nu_i(\mathcal{E}_i+\mathcal{E}_T)+\nu_{4s}\mathcal{E}_{4s}+\nu_{4p}\mathcal{E}_{4p}]$$

is a total loss per electron–ion pair created.[28,29] The latter includes power losses for ionization (first term), thermal motion and flows of plasma particles through the sheaths to the vessel walls (second term $\mathcal{E}_T=3T_e$) and excitation of neutral gas to $4s$ and $4p$ states (third and fourth terms, respectively). For the ionization and excitation rates in argon we have[28]

$$\nu_j = \alpha_j \times 10^8 T_e^{\zeta_j} p_0 \exp(-\mathcal{E}_j/T_e), \tag{12}$$

where $j=(i,4s,4p)$, $\alpha_i=8.13$, $\alpha_{4s}=1.77$, $\alpha_{4p}=4.95$, $\zeta_i=0.68$, $\zeta_{4s}=0.74$, and $\zeta_{4p}=0.71$. Here, $\mathcal{E}_i=15.76$ eV, $\mathcal{E}_{4s}=11.56$ eV, and $\mathcal{E}_{4p}=13.2$ eV are the ionization and excitation thresholds, respectively. In Eq. (12), T_e is in units of eV and p_0 is in Torr. In Eq. (11), $D_a \sim T_e \mu_i / e$ is the ambipolar diffusion coefficient, $\mu_i \sim e/m_i \nu_{\text{in}}$ is the ion mobility, and m_i is the ion mass. For the rate of ion–neutral collisions one has $\nu_{\text{in}}=N_n \sigma_{\text{in}} V_{Ti}$, where V_{Ti}, N_n, and σ_{in} are the ion thermal velocity, density of neutrals and the cross section for ion–neutral collisions, respectively. The pressure range below a few hundred mTorr is considered so that one can assume that the ambipolar diffusion is a dominant regime for the particle loss.[30]

In the boundary conditions for the electron/ion fluxes, we account for the finite width of the plasma sheath. Indeed, the radial $\Gamma_r=-D_a \partial n_e/\partial r$ and axial $\Gamma_z=-D_a \partial n_e/\partial z$ fluxes satisfy

$$\Gamma_r(r=R)=\Gamma_z(z=L)=\Gamma_z(z=0-)=n_s u_B$$

and

$$\Gamma_z(z=-\mathcal{L})=\Gamma_z(z=0+)=-n_s u_B,$$

where $u_B=(T_e/m_i)^{1/2}$ and n_s are the ion velocity and density at the sheath edge, respectively. The effective diffusion length $\Lambda=(\chi^2+\gamma_z^2)^{-1/2}$ corresponds to the stationary state of Eq. (11), when the spatially averaged ionization gain and ambipolar diffusion loss balance each other. The approximate plasma density profile is

$$n_e(r,z)=n_{e0} J_0(\chi r)\cos[\gamma_z(z-L/2)], \tag{13}$$

where T_e, χ, and γ_z satisfy $\gamma_z^2+\chi^2=\nu_i/D_a$, $\gamma_z \tanh(\gamma_z L/2)=u_B/D_a$, $\chi J_1(\chi R)/J_0(\chi R)=u_B/D_a$, and it is implied that $u_B \equiv u_B(T_e)$, $D_a \equiv D_a(T_e)$, and $\nu_i \equiv \nu_i(T_e)$.

The standard iteration procedure[17] allows one to obtain the electron temperature as a function of the working gas pressure and chamber sizes. We note that T_e declines in the pressure range 15–200 mTorr, which appears to be consistent with numerical and experimental results on rf discharges in argon.[23,24,31]

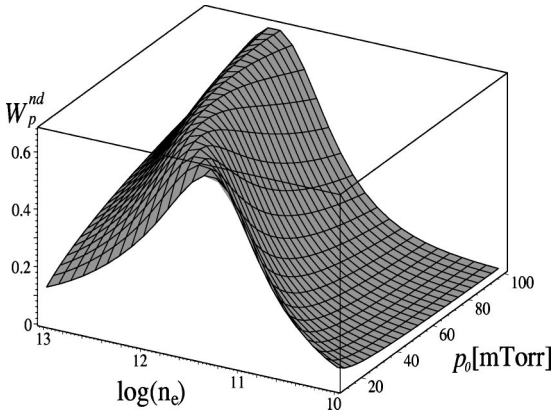

FIG. 10. 3-D plot of the dimensionless power transferred to plasma electrons vs plasma density and gas pressure.

V. DISCHARGE WORKING POINTS

We now estimate the minimum power deposition necessary to sustain the discharge and produce the desired plasma density. Figures 11 and 12 show the power absorbed W_p and lost W_{loss} by the electrons as a function of the plasma density

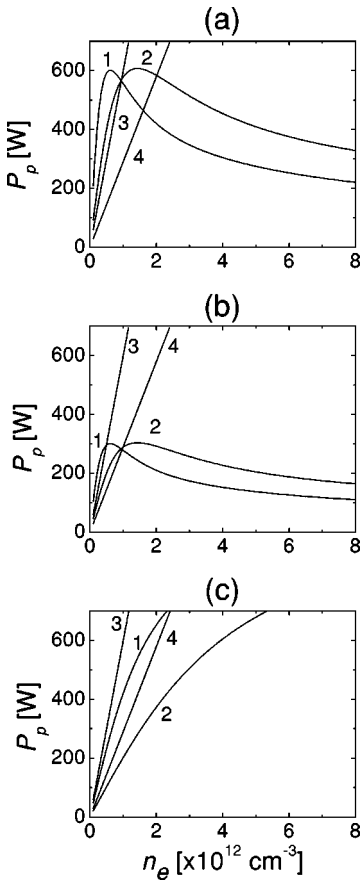

FIG. 11. P_p and P_{loss} as a function of argon plasma density for 30 and 70 mTorr IRCGPs (a), IOCGPs (b), and ICPs (c) with $I_0=$ 15 A.

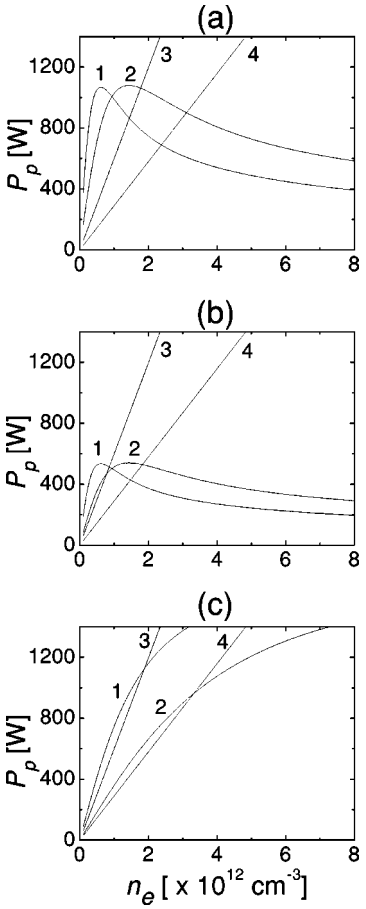

FIG. 12. Same as in Fig. 11, for $I_0 = 20$ A.

for different gas pressures and rf currents 15 A (Fig. 11) and 20 A (Fig. 12) driven in coils of different configurations. The intersection of power deposition and loss curves yields the minimum power necessary to sustain a discharge with the desired plasma density. As can be seen from Fig. 11 ($I_0 = 15$ A), the spatially averaged plasma density $n_e \sim 9.4 \times 10^{11}$ cm^{-3} can be produced in the IRC configuration at gas pressure $p_0 = 30$ mTorr with input power of ~ 570 W. Meanwhile, the IOCGP with density $n_e \sim 5 \times 10^{11}$ cm^{-3} can be generated with only ~ 295 W of rf power at the same gas pressure. One can notice that curves W_p and W_{loss} do not intersect in the ICP configuration for the coil current of 15 A.

Hence, under such conditions the conventional ICP configuration is not capable of generating a plasma. By raising the gas pressure, one can achieve higher plasma densities. For instance, at $p_0 = 70$ mTorr, 580 W of rf power can generate plasmas with $n_e \sim 2 \times 10^{12}$ cm^{-3} in the IRC configuration (IRCC), while a power of 291 W is sufficient to create the plasma with $n_e \sim 10^{12}$ cm^{-3} in the IOCC. As can be seen from Fig. 12, the ICP can only be produced by rf currents higher than 20 A. Indeed, at 30 mTorr, a power of 1125 W is necessary to sustain plasmas with $n_e \sim 1.9 \times 10^{12}$ cm^{-3} in this configuration at $I_0 \sim 20$ A. In the IOC and IRC configurations such values are $n_e \sim 1.4 \times 10^{12}$ cm^{-3} with ~ 870 W, and $n_e \sim 8.6 \times 10^{11}$ cm^{-3} with ~ 520 W, respectively.

At $p_0 = 70$ mTorr, the electron number density can be as high as 3.1×10^{12} cm^{-3} in the IRCC, 1.8×10^{12} cm^{-3} in the IOCC, and 3.3×10^{12} cm^{-3} in the ICP. The rf power required to sustain the plasma column amounts to ~ 900, ~ 530, and ~ 963 W, respectively. The rf discharge working points corresponding to different coil configurations and operating gas pressures are summarized in Table II. It is worth emphasizing that the plasma cannot be generated in the ICPC at coil currents lower than ~ 20 A. However, the IRC and IOC configurations can produce dense plasmas even at coil currents as low as ~ 10 A.

TABLE II. Discharge working points.

Configuration and gas pressure (mTorr)	n_e (cm^{-3})	P_p (W)
$I_0 = 18$ A		
IOC, 20	4.9×10^{11}	423.78
IOC, 30	7.2×10^{11}	429.59
IOC, 50	1.1×10^{12}	434.24
IOC, 70	1.5×10^{12}	436.56
IOC, 100	2.0×10^{12}	438.89
IRC, 20	8.5×10^{11}	733.63
IRC, 30	1.3×10^{12}	745.26
IRC, 50	2.0×10^{12}	761.53
IRC, 70	2.7×10^{12}	775.45
IRC, 100	3.6×10^{12}	787.10
ICP, 20	7.6×10^{11}	670.77
ICP, 30	1.0×10^{12}	616.72
ICP, 50	1.2×10^{12}	477.73
$I_0 = 20$ A		
IOC, 20	5.8×10^{11}	507.69
IOC, 30	8.5×10^{11}	515.44
IOC, 50	1.4×10^{12}	524.74
IOC, 70	1.8×10^{12}	529.39
IOC, 100	2.5×10^{12}	534.04
IRC, 20	9.8×10^{11}	853.19
IRC, 30	1.4×10^{12}	866.75
IRC, 50	2.3×10^{12}	888.45
IRC, 70	3.1×10^{12}	902.01
IRC, 100	4.2×10^{12}	921.00
ICP, 20	1.3×10^{12}	1152.40
ICP, 30	1.9×10^{12}	1124.60
ICP, 50	2.7×10^{12}	1041.21

VI. DISCUSSION

We have investigated the effect of a spatially invariable (unidirectional) internal rf current on ICPs sustained in a cylindrical metal vessel. The implications and limitations of this study will be discussed in this section. Physically, the introduction of an oscillating rf current inside the vacuum chamber significantly affects the electromagnetic field distribution, rf power deposition and modifies the parameters of the plasma produced. The simplified approach adopted here involves consideration of both electrodynamics and power/particle balance. The electromagnetic field profiles and the rf power density are computed using an assumption about the spatial uniformity of the plasma density in the chamber. The output of the electrodymanic analysis is used to calculate the working points of the discharge, where

$$n_v = V_p^{-1} \int_{V_p} n_e \, dV$$

is the electron/ion number density averaged over the plasma volume V_p, which was approximately taken as the chamber volume. Thus, the results for the electromagnetic field profiles correspond to a uniform plasma density equal to the spatially averaged one n_v.

Driving the oscillating rf current inside the chamber one can achieve substantially better uniformity of power deposition near the chamber axis, as compared with the ICP devices with an external flat spiral coil. The specific configuration of I_{RF} allows one to achieve an azimuthally profiled distribution of the power density, which is similar to that in dipolar ($m=1$) surface-wave-sustained plasma columns.[32] Furthermore, the rf azimuthal magnetic field H_ϕ generated by the IOC can restrain the radial and axial diffusion of electrons, thus affecting the corresponding plasma density profiles. Noting that H_ϕ is maximal at $\phi=0$ and vanishes at $\phi=90°$ Eq. (5), we infer that the electron diffusion is predominantly restrained in the cross sections with smaller values of ϕ. Hence, one should expect a gradual increase of the electron/ion number density with the variation of the azimuthal angle from 90° to 0°, the latter being the direction of the internal oscillating current. This may have important practical implications, such as fabrication of thin optical coatings with azimuthally profiled refractive index for spectral/polarization devices.[33]

Therefore, one can expect that the azimuthal variation of W_p will result in spatial nonuniformity of the ionization source, and hence, the electron temperature. In particular, this can lead to heat flows $Q=(5n_eT_e/2m_e\nu_{\mathrm{en}})\nabla T_e$ that can substantially modify the power balance in the discharge and be the reason for frequently observed deviations of the electron/ion number density profiles from the ones obtained from the conventional diffusion theory Eq. (13). The effect of nonuniformities in T_e and ionization rates on large-area rf plasmas in high aspect ratio ($R/L\sim1$) cylindrical chambers is the subject of a separate investigation.[34] For simplicity, the consideration in this work was limited to visualization of profiles of the rf power deposition and computation of the discharge working points in terms of the spatially averaged plasma density *versus* argon pressure. The model can further be improved by applying difference schemes[35] and a time-variable numerical approach[34] involving a crosslink between the electrodynamic and power/particle balance blocks. In this way, it might appear possible to obtain more realistic [than Eq. (13)] density profiles.

It is worthwhile to mention that our preliminary experimental results suggest that assumption of uniform radial and axial electron/ion density profiles is fairly accurate except for the narrow near-coil and near-wall regions,[36] which justifies the viability of the simple model adopted. The experiments are in progress and a report is expected in the near future.

In the above, the discharge operating points (Figs. 11 and 12) were computed for the two values of the gas pressure, namely 30 and 70 mTorr. Note that the intermediate (20–100 mTorr) pressure range is typical for a large number of processes including barrier layer deposition, passivation, photoresist striping in ultralarge scale integrated (ULSI) technologies, chemical vapor deposition of carbon-based films for data storage, wear-resistant, highly transparent coatings, synthesis of carbon nanotubes, quantum dots and nanoparticles.[1,3,6] In this pressure range, one can expect that collisional (ohmic) heating is a major power transfer channel, ambipolar diffusion being a major particle loss mechanism. However, at pressures below 10 mTorr, ubiquitous for deep micron ultrafine etching in ULSI manufacturing,[3] our model would be less accurate due to the increasing role of nonlocal (collisionless) dissipative low-pressure effects.[37]

The estimate below shows that the relative contributions of nonlocal (collisionless) power transfer effects amount to approximately 9% and 6% at 30 and 70 mTorr, respectively, and our assumption about the dominance of a collisional (ohmic) mechanism is fairly accurate. Indeed, the rates of electron–neutral collisions at 30 and 70 mTorr and $T_e\sim2.5$ eV amount to 2.12×10^8 and 4.94×10^8 s^{-1}, respectively. The approximate rate of nonlocal rf power transfer can be estimated by noting that the electron thermal velocity at $T_e=2.5$ eV is $V_{\mathrm{Te}}\sim6.17\times10^7$ cm/s. The rf field penetration length $(\gamma_1^{(2)})^{-1}$ appears to be 4 and 4.2 cm in the IOC plasmas sustained with $I_c=20$ A. In this case the plasma density is 8.5×10^{11} and 1.8×10^{12} cm^{-3}, respectively (see Table II for details). The average electron traverse time $\tau_e=V_{\mathrm{Te}}\gamma_1^{(2)}$ is thus 6.5×10^{-8} s^{-1} at 30 mTorr and 6.8×10^{-8} s^{-1} at 70 mTorr, respectively. Hence, $\tau_e\ll T_{\mathrm{rf}}$, where $T_{\mathrm{rf}}=2\pi/\omega$, and the rate of nonlocal (collisionless) electron heating can be approximated as $\nu_{\mathrm{st}}=V_{\mathrm{Te}}/2\Delta$, where $\Delta=(c/\omega_{\mathrm{pe}})\times(V_{\mathrm{Te}}/\pi\omega)^{1/3}$.[2,26] Accordingly, we have $\nu_{\mathrm{st}}^{(30\ \mathrm{mTorr})}=3.21\times10^7$ s^{-1}, whereas $\nu_{\mathrm{st}}^{(70\ \mathrm{mTorr})}=4.94\times10^7$ s^{-1}. The relative contribution of the nonlocal electron heating mechanism $\nu_{\mathrm{st}}/(\nu_{\mathrm{st}}+\nu_{\mathrm{en}})$ appears to be 0.09 and 0.06 at 30 and 70 mTorr, respectively. However, at low pressures (<10 mTorr), nonlocal heating can prevail over the ohmic one and has to be thoroughly accounted for in improved discharge models.

The other issue to be investigated is the rf magnetic field penetration due to essentially nonlinear effects.[8,38,39] In fact, this effect can further improve uniformity of the generation of rf currents throughout the chamber volume. Physically, in the planar external-coil ICP geometry the nonlinear poloidal currents j_{er} and j_{ez} generate a strongly nonlinear azimuthal magnetic field B_ϕ, which has no fundamental-frequency Fourier component.[39] This effect has recently been confirmed experimentally.[25] One can thus expect that the nonlinear plasma response at higher frequencies will also persist in the IOC configuration. Above all, finite B_ϕ can result in enhanced penetration of the rf field due to secondary nonlinear effects,[39] which become more pronounced at lower operation frequencies.[23]

The interesting feature of the IOC configuration is that the poloidal rf current and hence, the azimuthal magnetic field, are driven in a linear fashion at the fundamental frequency and one can expect enhanced rf field penetration due to *primary* nonlinear effects. Furthermore, the internal oscillating current eliminates the nonuniformity of the rf power density in the vicinity of the chamber axis, which is inherent to the flat external coil ICP configurations.[15]

From a practical point of view, the IOC can easily be generated by a sole rf generator, which can be regarded as an advantage over the well-established IRC scheme, which requires special sophisticated generators of rotating rf

currents.[19] In particular, the results on the oscillating magnetic field current drive in compact spherical tori[21] and preliminary experiments[36] allow us to be optimistic about the successful testing of the IOC principle in the near future.

VII. CONCLUSION

The ICPs sustained by internal rf unidirectional (with spatially invariable phase) currents have been investigated. The set of Maxwell's equations has been used for the computation of the electromagnetic field profiles in weakly ionized dense plasmas of the rf discharge in argon. The power transferred to the plasma electrons has been obtained assuming electron–neutral collisions as a main mechanism for power transfer and invoking the fluid plasma model. The global discharge model has been used to calculate the minimum rf power necessary to sustain the argon plasma with the desired density. The electromagnetic field distribution, the efficiency and uniformity of power deposition, as well as the plasma properties have been compared with those in the ICP sources with an external flat coil and the internal rotating current sources with the same geometrical sizes. It has been demonstrated that introducing the internal oscillating current significantly improves the radial uniformity of power density in the chamber and favors generation of high-density plasmas with lower rf power consumption. The configuration is promising for thin film processes that require azimuthal profiling of power deposition. Finally, the easy operational principle and handling allow one to expect that the effect of the unidirectional internal oscillating current on ICPs in a fully metal cylindrical chamber will be tested experimentally in the near future.

ACKNOWLEDGMENTS

Fruitful discussions with I. R. Jones are kindly appreciated. This work was partially supported by the AcRF Grant Nos. RP 4/99 SX and RP 2/00 XS and NTSB Project No. 012 101 00247 (Singapore) and the Australian Research Council. E.L.T. acknowledges financial support from the NTU Research Scholarship. K.N.O. thanks the Japan Society for the Promotion of Science for financial support and H. Sugai for hospitality at Nagoya University, Japan.

[1] *Plasma-Surface Interactions and Processing of Materials*, edited by O. Auciello, A. Gras-Marti, J. A. Valles-Abarca, and D. L. Flamm (Kluwer, Boston, 1990).
[2] M. A. Lieberman and A. J. Lichtenberg, *Principles of Plasma Discharges and Materials Processing* (Wiley, New York, 1994).
[3] C. Y. Chang and S. M. Sze, *ULSI Technology* (McGraw–Hill, New York, 1996).
[4] I. G. Brown, A. Anders, M. R. Dickinson, R. A. MacGill, and O. R. Monteiro, Surf. Coat. Technol. **112**, 271 (1999).
[5] J. Hopwood, C. R. Guarnieri, S. J. Whitehair, and J. J. Cuomo, J. Vac. Sci. Technol. A **11**, 152 (1993).
[6] *Nanotechnology Research Directions: Vision for Nanotechnology, Research, and Development in the Next Decade*, edited by M. C. Roco, S. Williams, and P. Alivisatos (Kluwer Academic, Amsterdam, 1999).
[7] J. H. Hopwood, Plasma Sources Sci. Technol. **1**, 109 (1992); J. H. Keller, *ibid.* **5**, 166 (1996).
[8] M. Tuszewski, Phys. Plasmas **5**, 1198 (1998).
[9] V. A. Godyak, R. B. Piejak, B. M. Alexandrovich, and V. I. Kolobov, Phys. Plasmas **6**, 1804 (1999).
[10] I. M. El-Fayoumi and I. R. Jones, Plasma Sources Sci. Technol. **7**, 162 (1998); **7**, 179 (1998).
[11] M. Tuda, K. Nishikawa, and K. Ono, J. Appl. Phys. **81**, 960 (1997); P. L. G. Ventzek, T. J. Sommerer, R. J. Hoekstra, and M. J. Kushner, Appl. Phys. Lett. **63**, 605 (1993).
[12] G. Cunge, B. Crowley, D. Vender, and M. M. Turner, Plasma Sources Sci. Technol. **8**, 576 (1999); G. G. Lister and M. Cox, *ibid.* **1**, 67 (1992).
[13] S. Takechi and S. Shinohara, Jpn. J. Appl. Phys., Part 2 **38**, L148 (1999).
[14] M. Tuszewski, I. Henins, M. Nastasi, W. K. Scarborough, K. C. Walter, and D. H. Lee, IEEE Trans. Plasma Sci. **26**, 1653 (1998); M. Tuszewski, *ibid.* **27**, 68 (1999).
[15] Y. Wu and M. A. Lieberman, Appl. Phys. Lett. **72**, 777 (1998); Plasma Sources Sci. Technol. **9**, 210 (2000).
[16] S. S. Kim, H. Y. Chang, and C. S. Chang, Appl. Phys. Lett. **77**, 492 (2000).
[17] E. L. Tsakadze, K. N. Ostrikov, S. Xu, I. R. Jones, R. Storer, M. Y. Yu, and S. Lee, Phys. Rev. E **63**, 046402 (2001).
[18] I. R. Jones, C. Deng, I. M. El-Fayoumi, and P. Euripides, Phys. Rev. Lett. **81**, 2072 (1998); I. R. Jones, Phys. Plasmas **6**, 1950 (1999).
[19] G. Cottrell, I. R. Jones, S. Lee, and S. Xu, Rev. Sci. Instrum. **62**, 1787 (1991).
[20] K. Suzuki, K. Nakamura, H. Ohkubo, and H. Sugai, Plasma Sources Sci. Technol. **7**, 13 (1998).
[21] S. Xu, W. Luo, K. N. Ostrikov, J. Ahn, and S. Lee, Plasma Phys. Controlled Fusion **42**, 807 (2000); D. Brotherton-Ratcliffe and R. Storer, *ibid.* **31**, 615 (1989).
[22] J. D. Jackson, *Classical Electrodynamics* (Wiley, New York, 1967).
[23] S. Xu, K. N. Ostrikov, W. Luo, and S. Lee, J. Vac. Sci. Technol. A **18**, 2185 (2000).
[24] K. N. Ostrikov, S. Xu, and M. Y. Yu, J. Appl. Phys. **88**, 2268 (2000).
[25] S. Xu, K. N. Ostrikov, Y. Li, E. L. Tsakadze, and I. R. Jones, Phys. Plasmas **8**, 2549 (2001).
[26] V. Vahedi, M. A. Lieberman, G. DiPeso, T. D. Rognlien, and D. Hewett, J. Appl. Phys. **78**, 1446 (1995).
[27] A. B. M. Shafiul Azam, E. L. Tsakadze, Y.-A. Li, K. N. Ostrikov, S. Xu, and S. Lee, Bull. Am. Phys. Soc. **45**, 148 (2000).
[28] S. Ashida, C. Lee, and M. A. Lieberman, J. Vac. Sci. Technol. A **13**, 2498 (1995).
[29] F. Vidal, T. W. Johnston, J. Margot, M. Chaker, and O. Pauna, IEEE Trans. Plasma Sci. **27**, 727 (1999).
[30] Yu. P. Raizer, *Gas Discharge Physics* (Springer, Berlin, 1991).
[31] C. Lee and M. A. Lieberman, J. Vac. Sci. Technol. A **13**, 368 (1995).
[32] Yu. M. Aliev, H. Schlueter, and A. Shivarova, *Guided-Wave-Produced Plasmas* (Springer, Heidelberg, 2000).
[33] *Photonic Probes of Surfaces. Electromagnetic Waves: Recent Developments in Research*, edited by P. Halevi (Elsevier, Amsterdam, 1995).
[34] I. B. Denysenko, A. V. Gapon, N. A. Azarenkov, K. N. Ostrikov, and M. Y. Yu, Phys. Rev. E (submitted).
[35] S. K. Godunov and V. S. Ryabenkii, *Difference Schemes: An Introduction onto Underlying Theory* (North-Holland, Amsterdam, 1987); H. M. Wu, B. W. Yu, A. Krishnan, M. Li, Y. Yang, J. P. Yan, and D. P. Yuan, IEEE Trans. Plasma Sci. **25**, 776 (1997).
[36] E. L. Tsakadze, Z. L. Tsakadze, K. N. Ostrikov, and S. Xu (unpublished).
[37] V. A. Godyak, in *Electron Kinetics and Applications of Glow Discharges*, edited by U. Kortshagen and L. Tsendin (Plenum, New York, 1998), p.241.
[38] A. I. Smolyakov and I. Khabibrakhmanov, Phys. Rev. Lett. **81**, 4871 (1998).
[39] A. I. Smolyakov, V. Godyak, and A. Duffy, Phys. Plasmas **7**, 4755 (2000).